Efficiency evaluation of a ductless Archimedes turbine: Laboratory experiments and numerical simulations

Efficiency evaluation of a ductless Archimedes turbine: laboratory experiments and numerical simulations

Zitti Gianluca[a], Brocchini Maurizio[a], Fattore Fernando[b], Brunori Alessandro[c], Brunori Bruno[c]

[a]*Dipartimento di Ingegneria Civile, Edile e di Architettura (DICEA), Universitá Politecnica delle Marche, Ancona, Italy*
[b]*Neferti S.r.L. Milano (Consultant for), Milano, Italy*
[c]*Neferti S.r.L. Milano, Milano, Italy*

Abstract

The aim of designing a new hydrokinetic turbine simple, cheap, enviromentally friendly and suitable for remote areas is pursued by studing the efficiency of an Archimedes turbine, exploiting the kinetic energy rather than a difference in water head. First, the efficiency of a hydrokinetic Archimedes turbine is studied using laboratory experiments for low TSR regime. Subsequently, numerical simulations are run to evaluate the performance coefficient of the turbine only (without frictional losses or blockage augmentation), and to extend the TSR range. Numerical simulations lead to the determination of the efficiency curve of an hydrokinetic Archimedes turbine in aligned and inclined configuration. The obtained maximum performance coefficients are compared with the ones of other hydrokinetic turbines actually in use and exploited with parametric analysis to investigate the feasibility of the proposed turbine in real applications.

Keywords: Renewable energy, Hydrokinetic turbine, Archimedes turbine, efficiency evaluation, cheap installation

List of symbols

A	Cross section of the rotor
b	Width of the channel
C_p	Performace coefficient
$C_{p,t}$	Performace coefficient of the turbine only
f	Friction coefficient between teflon support device and steel joint

F_f Friction force on the turbine support devices
F_s Reactive force on the turbine support devices
g Gravitational acceleration
h Water depth
h_t Height of the turbine axis from the bottom
i Flume inclination
l Lenght of the experimental flume
L Lenght of the turbine
m Mass of the counterweight system
M_t Torque with respect to the turbine axis
p Stride lenght of the turbine
P_{diss} Dissipated power
P_f Fluid flow power
P_t Power generated by the turbine
Q flow rate in the channel; the subscripts *rect* and *circ* indicate the evaluation with the rectangular and circular spillways.
r Pulley radius at the turbine axis
r_i Radius of the i-th support devices
R Externaal radius of the turbine
s Displacement of the counterweight mass
v Tangental velocity of the pulley at the tubine axis, and average counterweight mass lift velocity
v_{in} Stream flow velocity
α Inclination of the blade with respect to the axis turbine
Δt Time steps for the measurement of the vertical mass displacement in experiments
η_e Performace coefficient of the generator or alternator
η_f Performace coefficient of the transmission and support system
ρ Density of the fluid
θ Angle of the turbine axis with the flow
ω Angular velocity of the turbine

1. Introduction

One fundamental societal challenge for the coming decades is the use of renewable energy resources, towards sustainable development [1]. Hydrokinetic turbines is a very promising tools towards such goal, with reference to all aspects (environmental, economic and social) of sustainable development, since they can produce energy through sustainable consumption of natural resources. In this context, the design of new hydrokinetic energy conversion system is of great interest.

Vermaak et al. [2] highlighted the tecnical, economical and environmental benefits of the micro-hydrokinetic river technology, which are able to operate with little or no water super-elevation. To evaluate the best option for rural electricity supply, a simulation program was used in [3, 4], comparing hydrokinetic power with wind, photovoltaic and diesel generator. Hydrokinetic power was found to be the best option, where water resources were available, being cost effective and reducing the CO_2 input in the atmosphere. Therefore, these renewable technologies provide a cost effective source of electricity in rural areas, where distances are large, population are small and demand for energy is low. Moreover, small hydrokinetic power systems reduce the number and size of the typical required infrastructures of hydropower plants (as described in [5]). The absence of these permanent infrastructures 1) reduces the impacts on the ecosystem and 2) facilitates the installation and mantainance in remote areas.

Various reviews on hydrokinetic power systems are available. For example, [6] and [7] provided an overview of vertical axis and horizontal axis hydrokinetic turbines; Kumar and Sarkan [8] reviewed a wider number of hydrokinetic energy conversion systems; Rostami and Fernandez proposed a vertical flat plate, free to rotate about a vertical axis of symmetry, to exploit the autorotation induced by the vortex shedding [9]; Finally, a review of vertical-axis autorotation current turbines is reported in [10].

In this context, the Archimedes screw turbine can have an important role. It has been longtime used in micro hydropower plants, with very high efficiencies (up to 85%, as reported in [11], where a traditional system is described), but it was classified as a reaction turbine different from hydrokinetic turbines in the review of Okot [12]. In fact, it exploits the potential energy gradient between two reservoirs and has never been employed in free flows. In view of its high performance, it was also applied in ducted systems. For example, Rigling, Schleicher and co-workers evaluated numerically the efficiency of a non-uniform Archimedean spiral rotor in [13], finding the best hydraulic efficiency point equal to 72%. In both traditional and ducted conditions, the system requires a set of structures, this constituting a significant enviromental impact and making the use of such technology in remote areas inconvenient.

The aim of our contribution is to investigate the possible use of the Archimedes screw turbine as an axial hydrokinetic turbine, i.e. arranging the screw in the fluid flow without any supply or protection system, in order to make the most of advantages of the hydrokinetic turbines described above. The use and optimization of an Archimedes screw as an hydrokinetic turbine comes from an idea of Soc. Neferti Srl, which designed and realized several prototypes of this kind of Archimedean-Type Hydrokinetic turbines. Field tests showed interesting responses and suggested a rigorous study of the turbine by means of more controllable laboratory and numerical simulations. The study, carried out by the Hydraulic research group of the Polytechnic University of Marche, aimed to evaluate the performance of the machine and to optimize the fundamental design parameters. The idea of an effective Archimedes hydrokinetic turbine aims at producing a device that: 1) is simple and cheap, therefore it can be used in remote areas and developing countries; 2) minimizes all environmental impacts; 3) does not require the construction of civil infrastructures (intake and discharge reservoirs, by-pass channels, etc.); 4) works also in channels and rivers with small water depths and 5) maximizes the flow energy exploitation.

Literature on hydrokinetic Archimedes turbines is very poor. A first attempt of using Archimedes screw as hydrokinetic turbine was proposed by Stergiopoulou and co-workers [14, 15, 16], but their works did not provide an accurate efficiency evaluation of the Archimedes screw hydrokinetic turbine or compared it with other hydrokinetic turbines. For that reason, in this paper we provide a more robust experimental and numerical study for the evaluation of the performances of a ductless two strides Archimedes turbine, analyzing different performance contributions and following rigorously the theory of hydrokinetic turbines. In particular, we consider the geometry of a classical Archimedes screw, slightly modified by inclining the blades toward the incoming flow, to optimize the harnessing of the flow power. The study makes use of both laboratory experiments and CFD numerical simulations, the latter being used to determine carefully the torque generated by the flow on an Archimedes screw turbine. Since technical requirements could involve the inclination of the turbine with respect to the flow, two different configurations (aligned with the flow and inclined with the flow) have been reproduced to understand which configuration provides the greater efficiency.

2. Hydrokinetic turbine efficiency

The use of the Archimedes screw turbine as an axial hydrokinetic turbine totally changes its operation principles: traditional Archimedes screw turbine exploits the difference in potential energy between two water reservoirs, whereas hydrokinetic turbines exploit the kinetic energy of the flow. Notwithstanding the geometrical differences among the various hydrokinetic turbines, the evaluation of the efficiency of an hydrokinetic turbine is based on Betz' one-dimensional model [17, 18], reported in Figure 1. Betz' model

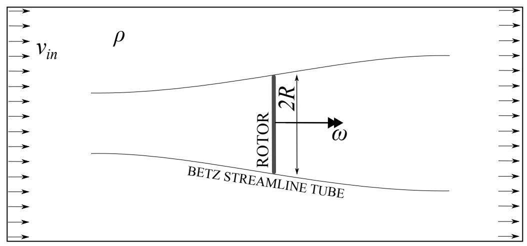

Figure 1: Sketch of Betz' model.

is composed by an ideal planar circular turbine with, radius R, crossed by an incompressible fluid flow with rectilinear streams of constant velocity, that leads to a rotation of the turbine with angular velocity ω. For such theory, the power available from the fluid flow P_f is:

$$P_f = \frac{1}{2}\rho A v_{in}^3 \tag{1}$$

where ρ is the fluid density, A is the cross flow area of the turbine and v_{in} is the stream flow velocity. The performance coefficient is given by the ratio $C_p = P_t/P_f$, where P_t is the power generated by the screw turbine. On the basis of Betz' theory, the performance coefficient has an upper limit of 0.59, but in practice several loss contributions reduces the efficiency of the turbines [19]. Betz' theory is widely used to evaluate the performance coefficient for wind turbines and commonly used also for more complex, three dimensional turbines. It was used in [20] to evaluate the efficiency of energy conversion systems that use water currents, and in [21] as basis for a comparative evaluation of different control schemes of hydrokinetic energy conversion systems. Another interesting example is given by Schleicher et al. [22], which used both experimental and numerical simulation to design a portable micro-hydrokinetic turbine, evaluating the efficiency by means of the Betz theory.

In general, the performance coefficient is related to three main contributions: the performace related to the turbine characteristics $C_{p,t}$, the losses related to the friction of the transmission and support system η_f, and the electrical losses in the generator or alternator η_e:

$$C_p = C_{p,t}\eta_f\eta_e \tag{2}$$

The performance coefficient C_p represents the dimensioness form of the turbine power production P_t, which depends on the turbine tip speed, i.e. on the rotation velocity and radius of the turbine. The correspondent dimensionless velocity is given by the ratio $TSR = \omega R/v_{in}$ (Tip Speed Ratio), where ω is the rotor angular velocity and R is the rotor diameter. As function of the TSR, the performance coefficients collapse onto a curve (of course, as long as the geometry and the Reynolds number range of the flow are the same). The performance coefficient curves of some turbines as function of the Tip Speed Ratio are available in [19].

Usually, the turbine performance coefficient is evaluated by measuring the power produced by the generator thus including all the three loss contributions of above. Here we focus on the performance coefficient of the turbine alone, using two different approaches: laboratory experiments and numerical simulations. Experiments are designed to avoid electrical losses, but an estimation of frictional losses is still required. Numerical simulations allow us to evaluate the power generated by the turbine alone, providing the turbine performance coefficient $C_{p,t}$.

In our laboratory experiments (see Figure 2 for a sketch of the experimental setup) the generated power was measured by a counterweight system, connected to the turbine axle, that slows down the turbine rotation. The power generated by the screw turbine P_t is obtained multiplying the counterweight force by the displacement velocity due to the turbine rotation. Then, the resultant performance coefficient obtained from the laboratory experiments is

$$C_{p,exp} = C_{p,t}\eta_f \tag{3}$$

where electrical losses are missing ($\eta_e = 1$), but frictional losses due to the support and counterweight systems must be evaluated to get the turbine efficiency alone.

On the other hand, numerical simulations provided a large amount of information on the flow surrounding the turbine, among which the resultant torque of the fluid pressure and the tension on the turbine surface. The product of the torque by the angular velocity gave the generated power and dividing this by the available fluid power we got the performance coefficient of the turbine alone:

$$C_{p,num} = C_{p,t} \tag{4}$$

3. Laboratory experiments

The experimental apparatus (see sketch in Figure 2) was composed by an open channel with small longitudinal slope, of lenght l=8 m, width b=0.3 m and height of 0.3 m. The channel was made of painted steel and the sides of the flume were equipped with transparent plexiglass windows for optical measurements. The flow in the flume was generated by a pump that took water from the discharge tank and pumped it in the charge tank of the flume. The flume at one end is hinged to the discharge tank, while the other end is

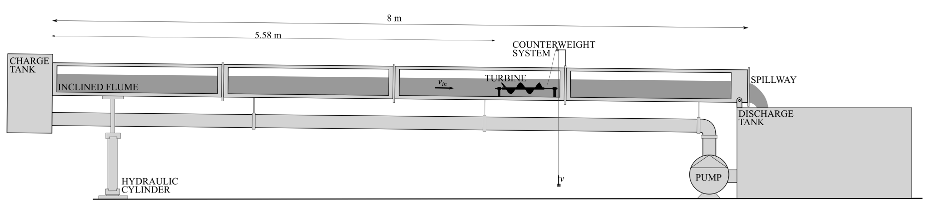

Figure 2: Sketch of the experimental setup.

supported by two hydraulic cylinders, that allow to vary the flume inclinaton between $i = 0\%$ and $i = 6.7\%$.

The fluid velocity v_{in} was varied by changing the flow rate in the channel and this was varied by controlling the longitudinal inclination of the flume and by using different types of spillway. The flume inclination was varied between $i = 0.48\%$ and $i = 2.04\%$ when using a circular spillway and between $i = 0.48\%$ and $i = 1.6\%$ when using a rectangular spillway. The flow rates were calculated by measuring the water depth at the spillway and using the spillway theory. The rectangular spillway (0.15 m wide and 0.1 high from the flume bottom) provided a flow rate of $Q_{rect} = 8.28 \cdot 10^{-3}$ m^{3}s^{-1}; the circular spillway (with diameter 0.15 m and height from the flume bottom of 0.1 m) provided a flow rate of $Q_{circ} = 7.60 \cdot 10^{-3}$ m^{3}s^{-1}. The water depth was measured for each inclination, but in the range of the used flume inclinations, the

Table 1: Flume configurations with corrisponding velocity and related available power P_f for the turbine in the cases aligned ($\theta = 0°$) and inclined ($\theta = 10°$) turbine.

ID	i [%]	Spillway	Q [m^{3}s^{-1}]	h [m]	v_{in} [ms^{-1}]	$P_{f,\theta=0}$ [mW]	$P_{f,\theta=10}$ [mW]
F1	0.48	Circular	$7.60 \cdot 10^{-3}$	0.206	0.1239	7.4692	12.6402
F2	0.96	Circular	$7.60 \cdot 10^{-3}$	0.195	0.1309	8.8080	14.9060
F3	1.6	Circular	$7.60 \cdot 10^{-3}$	0.179	0.1426	11.3872	19.2708
F4	2.04	Circular	$7.60 \cdot 10^{-3}$	0.17	0.1502	13.3067	22.5191
F5	0.48	Rectangular	$8.28 \cdot 10^{-3}$	0.187	0.1477	12.6532	21.4132
F6	0.96	Rectangular	$8.28 \cdot 10^{-3}$	0.177	0.156	14.9085	25.2298
F7	1.6	Rectangular	$8.28 \cdot 10^{-3}$	0.162	0.1704	19.4298	32.8813

flow rate did not vary with the inclination. For each configuration, the water depth h at several points along the water channel axis was measured and the section-averaged fluid velocity was evaluated as $v_{in} = Q/bh$. The location of the screw and the flume inclination have been chosen in order to have a water layer over the turbine at least 20 mm thick and as far as possible from the charge tank, in order to minimize its influence on the turbine. For these reasons the turbine has been placed 5.58 m downstream of the charge tank. The turbulence in the channel was not measured, but the Reynold number was estimated as $Re \geq 25000$ for all the configurations, then the flow was taken to be fully turbulent. The section-averaged flow velocities measured at the turbine location ranged between $v_{in} = 0.12$ and $v_{in} = 0.17$ ms^{-1} and are reported in Table 1, togheter with the other experimental characteristics. The power of the flow P_f has been evaluated with Eq. 1, where the rotor area A was approximated by the projection of the turbine volume on a plane perpendicular to the flow. In our case the turbine rotates inside a cilindrical volume of radius R and, if the axis of the turbine is parallel to the flow, the cross section area is that of a circle of radius R. If the angle of the turbine axis with the flow direction is $\theta \neq 0$, the cross section area is $A = R^2\pi \cos\theta + 2RL \sin\theta$, where L is the turbine lenght. Therefore, varying the angle θ, the flow power increases because of the increase in A. Also for this reason, the tests have been executed using two angles: $\theta = 0$ (aligned configuration) and $\theta = 10$ (inclined configuration). Larger angles have not been tested to avoid interactions of the lateral flow with the flume walls.

The design of screw turbine for laboratory experiments is inspired to the

Archimedean screw used in small hydropower plant, characterized by a scale of several meters (e.g [11]). Since the turbine object of this study is conceived for working without the construction of civil infrastructures, we can hypothesize that in a real application the dimension of the turbine depends on the size of the river and can range between some decimeters and several meters. Due to the geometrical geometrical of the laboratory flume, we design a turbine with radius 0.1 m and only two blade strides. The screw model (Figure 3) was made of an aluminium structural axle, to which the other parts were connected: the screw tubular axle and blades, the counterweight system, and the support devices (Figure 3a). The tubular cantilever,

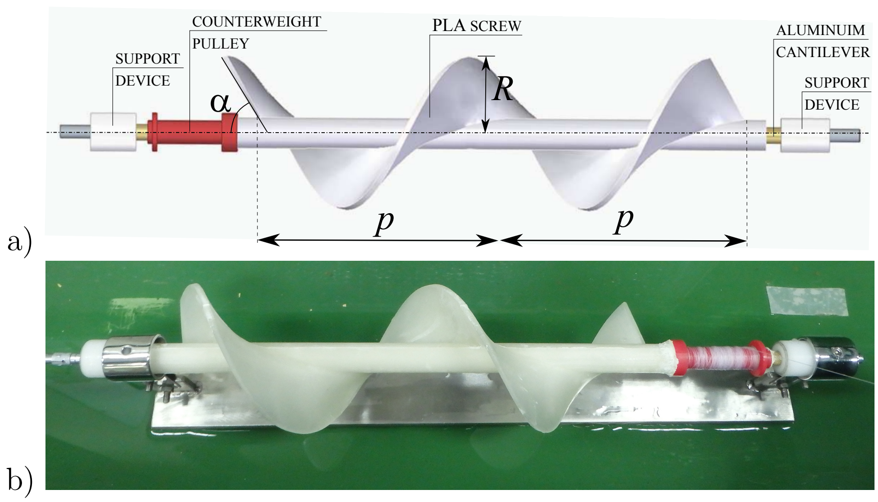

Figure 3: The screw turbine used for the experiments. a) sketch of the screw turbine model with main components; b) top view of the turbine in the support sistem.

with diameter 12 mm and thickness 1 mm, provided stiffness and resistence to the screw, which was realized in polylactic acid (PLA) with a 3D printer. The screw was composed by another tubular axle and a two strides blade. It was realized in two parts, which were glued together and with the structural part using an high performance glue. The screw PLA axle had diameter of 20 mm, while the blade was 5 mm thick, had external radius of $R = 50$ mm and each stride was long $p = 160$ mm. The blade was not perpendicular to the axle, but inclined of $\alpha = 70°$ with respect to the turbine axis, facing the incoming flow. A summary of the main geometry parameters of the tested turbine is reported in Table 2.

The support devices were two teflon cylinders, with diameter 27.5 and

Table 2: Geometry parameters of the turbine.

Parameter	symbol	value
Turbine radius	R	50 mm
Axle radius	-	20 mm
Axle length	L	320 mm
Blade stride	p	160 mm
Blade inclination with respect to axle	α	70°

30.5 mm, connected at the extremities of the structural tube, which could be lodged in a steel support system. The support system was made of a steel plate 10 mm thick, 600 mm long and 80 mm wide, holding two spigot joints by means of small spilled plates (see Figures 3b and 4). The leeside spigot joint was equipped with an additional internal small peg, which prevented the turbine from sliding along its axis and exiting the support system during operation. The support system allowed for rotation of the support devices (and subsequently of the turbine) and located the turbine axis at h_t=89 mm from the bottom of the flume. The friction between the support devices and the support system was not negligible, but it was reduced as much as possible by using a teflon-steel wet interface.

The structural axle was equipped with a pulley for the counterweight system (Figure 4), that was made of a string with negligible stiffness, fixed at the turbine pulley and holding a mass of $m = 9$ g. The string could overpass the flume wall by means of an additional pulley fixed to the flume itself. The distance between such pulley and the ground (i.e. the maximum excursion of the counterweight system) was 1.5 m.

At the beginning of each test the turbine was kept still and the counterweight mass held at few centimeters above ground. When the turbine was released the video camera started recording the displacement of the conterweight mass during all its excursion with a frequency of 29.97 frs^{-1}. A dark panel and a measuring tape were put behind the mass to regard the mass itself as a target and measure the displacement s of the mass at fixed time steps of $\Delta t = 250$, in which the video was divided. Then, the lift velocity for each time step was evaluated as $v = s/\Delta t$. An example, related to test F1-θ0 is reported in Table 3. No relevant acceleration was revealed by the sensitivity of the instrument, even if in some experiments the velocity fluctuated significantly. This suggested that the rotation of the turbine is not constant, but no clear trend was inferred from the entire experimental set. Hence, the time average

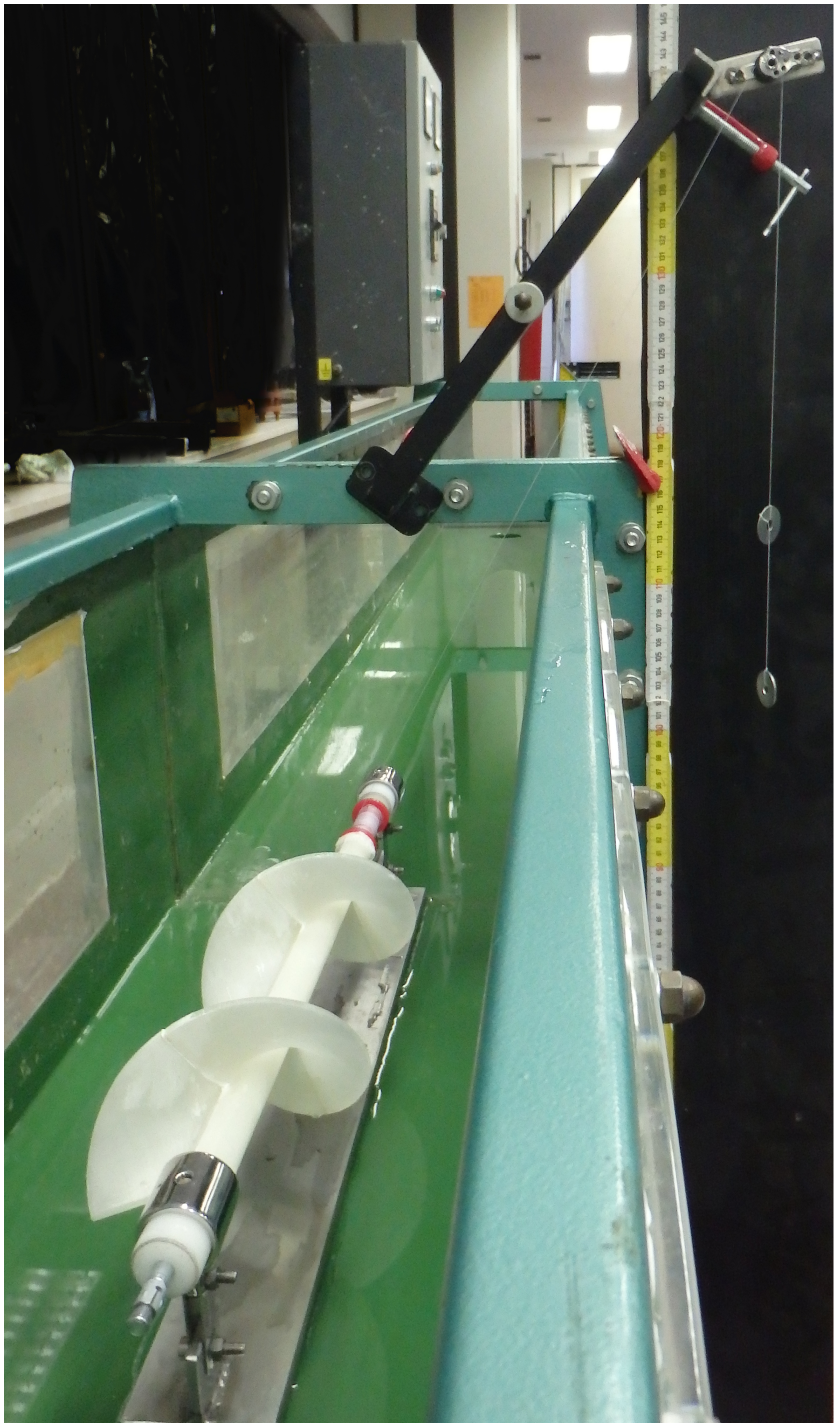

Figure 4: Perspective view of the turbine in the support system inside the flume, connected to the counterweight system (top right).

Table 3: Measured velocity for Test F1-$\theta 0$

t [fr]	v [ms^{-1}]
250	$1.435 \cdot 10^{-2}$
500	$1.252 \cdot 10^{-2}$
750	$1.121 \cdot 10^{-2}$
1000	$1.235 \cdot 10^{-2}$
1250	$1.560 \cdot 10^{-2}$
1500	$1.605 \cdot 10^{-2}$
1750	$1.547 \cdot 10^{-2}$
2000	$1.260 \cdot 10^{-2}$
2250	$0.963 \cdot 10^{-2}$
2500	$1.131 \cdot 10^{-2}$
2750	$1.135 \cdot 10^{-2}$
3000	$1.083 \cdot 10^{-2}$
3250	$1.080 \cdot 10^{-2}$
3500	$1.221 \cdot 10^{-2}$
3750	$1.119 \cdot 10^{-2}$
4000	$1.329 \cdot 10^{-2}$
4250	$1.025 \cdot 10^{-2}$

Table 4: Experimental confgurations and results.

ID	v_{in} [ms^{-1}]	v [ms^{-1}]	$\sigma(v)$ [ms^{-1}]	ω [rads^{-1}]	TSR [adim]	P_t [mW]	P_f [mW]	$C_{p,exp}$ [adim]	P_{diss} [mW]	$C_{p,t}$ [adim]
F1-θ0	0.1239	$1.249\cdot10^{-2}$	$1.02\cdot10^{-3}$	1.67	0.1008	1.103	7.469	0.148	0.819	0.257
F2-θ0	0.1309	$1.510\cdot10^{-2}$	$2.18\cdot10^{-3}$	2.01	0.1153	1.333	8.808	0.151	0.990	0.264
F3-θ0	0.1426	$1.636\cdot10^{-2}$	$1.34\cdot10^{-3}$	2.18	0.1147	1.444	11.387	0.127	1.073	0.221
F4-θ0	0.1502	$2.052\cdot10^{-2}$	$4.12\cdot10^{-3}$	2.74	0.1366	1.812	13.307	0.136	1.345	0.237
F5-θ0	0.1477	$1.333\cdot10^{-2}$	$0.81\cdot10^{-3}$	1.78	0.0903	1.177	12.653	0.093	0.874	0.162
F6-θ0	0.156	$1.557\cdot10^{-2}$	$1.52\cdot10^{-3}$	2.08	0.0998	1.375	14.908	0.092	1.021	0.161
F7-θ0	0.1704	$2.114\cdot10^{-2}$	$1.53\cdot10^{-3}$	2.82	0.1241	1.867	19.430	0.096	1.386	0.167
F1-θ10	0.1239	$0.964\cdot10^{-2}$	$0.69\cdot10^{-3}$	1.28	0.0778	0.851	12.640	0.067	0.632	0.117
F2-θ10	0.1309	$1.323\cdot10^{-2}$	$0.93\cdot10^{-3}$	1.76	0.1011	1.168	14.906	0.078	0.867	0.137
F3-θ10	0.1426	$1.613\cdot10^{-2}$	$1.51\cdot10^{-3}$	2.15	0.1131	1.421	19.271	0.074	1.058	0.129
F4-θ10	0.1502	$1.948\cdot10^{-2}$	$1.32\cdot10^{-3}$	2.60	0.1297	1.720	22.519	0.076	1.277	0.133
F5-θ10	0.1477	$1.543\cdot10^{-2}$	$1.21\cdot10^{-3}$	2.06	0.1045	1.363	21.413	0.064	1.012	0.111
F6-θ10	0.156	$1.937\cdot10^{-2}$	$1.42\cdot10^{-3}$	2.58	0.1242	1.710	25.230	0.068	1.270	0.118
F7-θ10	0.1704	$2.271\cdot10^{-2}$	$2.58\cdot10^{-3}$	3.03	0.1333	2.005	32.881	0.061	1.489	0.106

over the run duration of the measured lift velocity v was calculated. The average velocity measured with this procedure corresponded to the tangential velocity of the turbine pulley and was related to the turbine angular velocity ω through the relation $v = \omega r$, where $r = 7.5$ mm was the radius of the pulley where the string was rolled, at the turbine axis.

The system of above allowed one to evaluate the power generated when the turbine rotated, simply multiplying the weight force of the mass by the lift velocity:

$$P_t = mgv \tag{5}$$

where g was the gravitational acceleration.

Summarizing, 14 different experimental conditions were reproduced (see Table 4). Each test condition was reproduced three times to check its repeatability. The velocity averaged over such three realizations was used to evaluate the power generated P_t and, subsequently, the experimental performance coefficient $C_{p,exp}$. The results are summarized in Table 4, which also gives the angular velocity of the turbine ω and the TSR to be used for comparison with other hydrokinetic turbines.

To highlight trends in the performance coefficient, the experimental results have been divided into two groups, corresponding to the two different configurations (aligned and inclined), and the arithmetic means of TSR and $C_{p,exp}$ in each group has been calculated, providing TSR=0.1117 and $C_{p,exp} = 0.12$ for the aligned configuration and TSR=0.1112 and $C_{p,exp} = 0.07$ for the inclined configuration.

Power losses were due to the friction that developed along the contact surface between the moving body (teflon turbine support devices) and the fixed body (steel joints). The teflon-steel friction coefficient was taken equal to $f = 0.04$ (as reported in several engineers handbooks) and the friction force was estimated as $F_f = fF_s$, where F_s was the reaction force, equally divided between the two joints:

$$F_s = \frac{(m_t - \rho V_t)\, g}{2} \tag{6}$$

where $m_t = 0.325$ kg and $V_t = 0.239 \cdot 10^{-3}$ m^3 were the turbine mass and volume respectively, while ρ was the water density. The reaction force was always the same for all experiments $F_s = 0.42$ N and produced a friction force equal to $F_f = 16.96 \cdot 10^{-3}$ N. The friction force, tangential to the joint surfaces, dissipated a power equal to

$$P_{diss} = F_f \omega \, (r_1 + r_2) \tag{7}$$

where $r_1 = 0.01375$ m and $r_2 = 0,01525$ m were the radii of the two teflon support devices. The dissipated power is reported, for each test, in the penultimate column of Table 4. The sum of the measured power $P_{t,exp}$ and dissipated power P_{diss} provided an estimate of the turbine generated power that was used to evaluate the performance coefficient of the machine alone $C_{p,t}$ (Table 4) and to extrapolate the efficiency of the support system, which is $\eta_f = 0.574$ for all the experiments. Considering both the measured and dissipated power, the set-averaged performance coefficient of the machine alone was $C_{p,t} = 0.21$ for the aligned configuration and $C_{p,t} = 0.12$ for the inclined configuration.

4. Numerical simulations

A more accurate evaluation of the performance coefficient of the machine alone $C_{p,t}$ is possible by means of dedicated numerical simulations. CFD is often used in literature to evaluate the performace coefficient of several kinds of turbines (e.g.[13, 23]). In our case, we used CFD simulations to extrapolate the effect of the flow directly on the turbine, in terms of pressures and shear stresses and to evaluate the torque generated by the flow on the turbine. Numerical simulations have been performed by means of the Academic Ansys Fluent software, solving the Reynolds Averaged Navier Stokes equations on a fluid domain that reproduced the geometry of the experiments described in Section 3.

Since our goal was to evaluate the performance coefficient of the turbine alone, the geometry of the laboratory turbine was reproduced in detail, the support system and the countweight system were neglected and the flume were substituted by a fluid domain larger than that characterizing the laboratory experiments. This larger domain, with free slip boundary conditions, aim at removeing the effects of the walls, free surface and possible blockage effects. In this manner, numerical simulations provided results that could not be validated with experiments, but allowed us to focus on the power generation of the turbine only and extend the operative condition of the turbine to the entire possible range. In more detail, the fluid volume was a parallelepiped 2 m long in the streamwise direction, 1 m wide and 0.6 m high (a sketch of the horizontal plane of the domain for both configurations is reported in Figure 5). The turbine was located at the center of the crossflow section, at a distance of $4R$ from the inflow boundary and of $30R$ from the outflow boundary, to minimize the interaction of upstream and downstream hydrodinamic phenomena with the boundaries [24]. For the inclined turbine the same distances were used, the center of the turbine corresponding to the center of a crossflow section.

To generate a constant flow inside the domain the inflow-ouflow boundary condition were assigned at boundaries 1 (inflow) and 2 (outflow) of Figure 5. To simulate a condition similar to the experiments of Section 3, the velocity $v_{in} = 0.2$ ms^{-1} was assegned at both inflow and outflow boundaries. Free slip wall boundary condition were assigned at the other four boundaries.

The fluid domain used in the numerical simulations was divided into two parts, applying the multiple reference frame (MRF) method to include multiple rotating reference frames in a single domain (see Figure 5). The MFR method [25] included in a single domain multiple rotating reference frames, whose interface is chosen in such a way that the flow field at this location is independent of the orientation of the moving parts. The calculation domain is divided into subdomains, one of which is rotating with respect to the other (inertial) frame. The governing equations (mass conservation and momentum conservation) in each subdomain are written with respect to that subdomain's reference frame. At the boundary between two subdomains, the continuity of the absolute velocity is enforced to provide the correct neighbor values of velocity for the subdomain under consideration. The resulting flow field was representative of a snapshot of the transient flow field in which the rotating parts were moving.

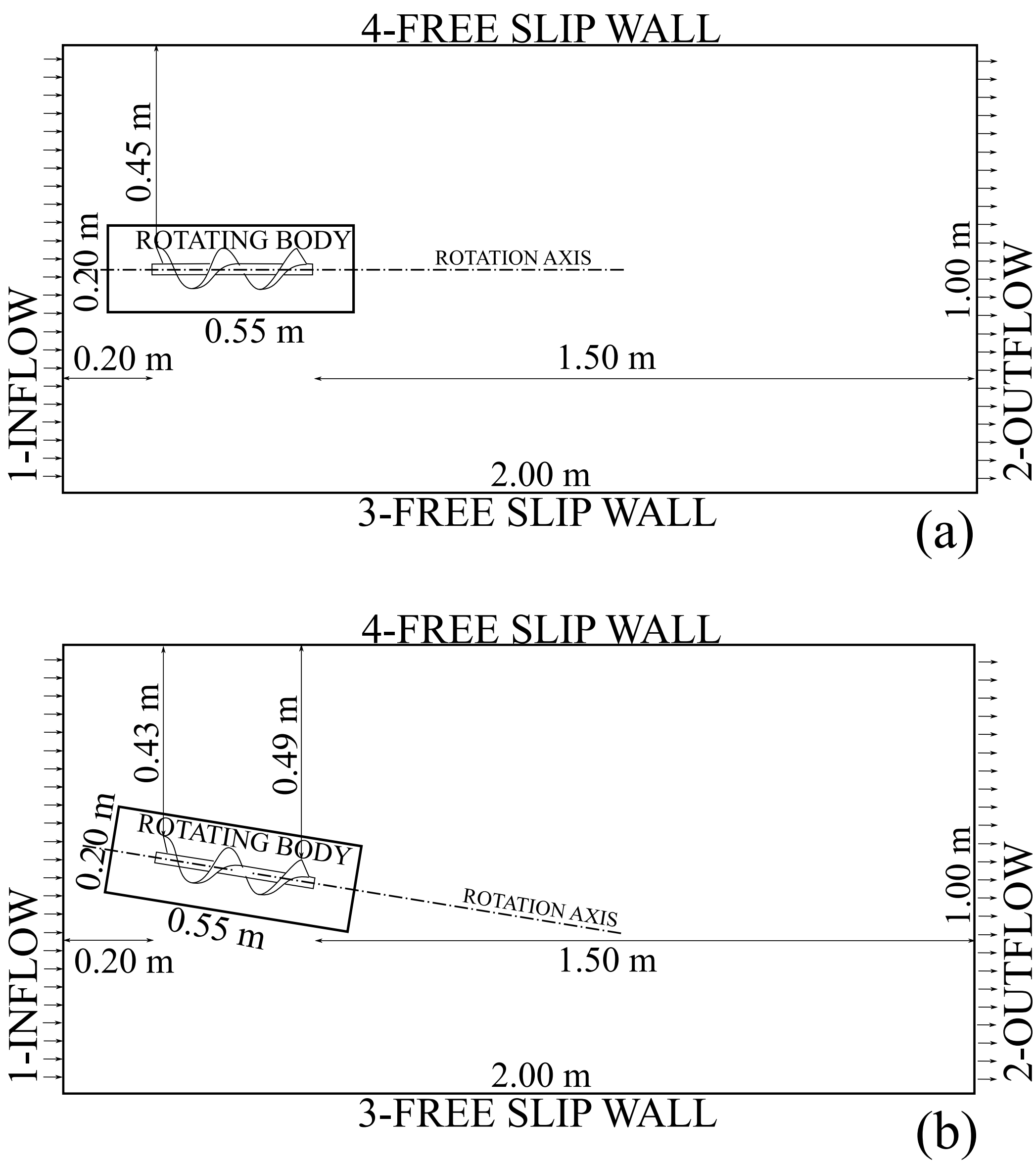

Figure 5: Sketch of the horizontal plane of the geomentry of the domains used in the numerical simulations. a) aligned turbine ($\theta = 0°$); b) inclined turbine ($\theta = 10°$).

For the problem under consideration, the rotating part of the domain, hereafter called the rotating body, was a cylindrical volume with radius twice the turbine diameter and lenght 0.55 m, which contained the turbine and had the same axis of the turbine. The rest was the complementary to the parallelepiped fluid domain. The mesh was generated separately in the two parts and the rotation of the turbine was simulated moving the rotating body at each time step with an assigned angular velocity ω. The solutions of the two domains were calculated in the different reference frames for each part and the boundary condition for the inner rotating body were evaluated by interpolation on the outer body mesh.

The mesh, generated with Ansys Meshing Tool (ICEM CFD), was composed of linear tetrahedical cells, with maximum size of $3 \cdot 10^{-2}$ m. Since the focus of the simulation is the evaluation of the interaction forces on the turbine walls, the mesh was refined on the surface of the screw. On the turbine surface the mesh size was assigned equal to $3 \cdot 10^{-3}$ m, with an inflation perpendicular to the wall that assigned a first layer thickness equal to $1 \cdot 10^{-4}$ m and increased gradually the thickness for twelve layers around the turbine, with a growth rate of 1.4. A representation of the refinement is given in Figure 6. The above procedure led to a mesh of 157.111 nodes and 529.599 cells for the flow-aligned turbine and a mesh of 141.946 nodes and 527.710 cells for the $10°$ inclined turbine. The first layer inflation at the screw wall was assigned to ensure a dimensionless wall distance $y^+ < 5$, as suggested in [26] for $k-\omega$ Shear Stress Transport ($k-\omega$ SST) model. Because the complex geometry prevented us from doing a previous estimation of the velocity gradient at the wall, the value of y^+ was evaluated a posteriori for each simulation, finding a y^+ smaller than 4 for all the simulations, this respecting the suggested limit of $y^+ < 5$.

The numerical model was a pressure-based model that solved the discretized form of the Reynolds Averaged Navier Stokes Equation. The turbulence model used to close the equations was the Menter's $k-\omega$ Shear Stress Transport ($k-\omega$ SST) model, which works well with adverse pressure gradients and separating flow (see [27, 28, 26] for details). Some examples for the application of this model, also for different condition, are given by [29, 30]

The two geometries of Figure 5 were used to run several simulations, differing in the angular velocity of the turbine, in order to range the TSR and evaluate the performance curve of the turbine for the two different configurations. For each configuration, the angular velocity of the turbine was varied from 0.5 to 6 rads^{-1}, with steps of 0.5 rads^{-1}. Since the flow velocity is $v_{in} = 0.2$ ms^{-1},

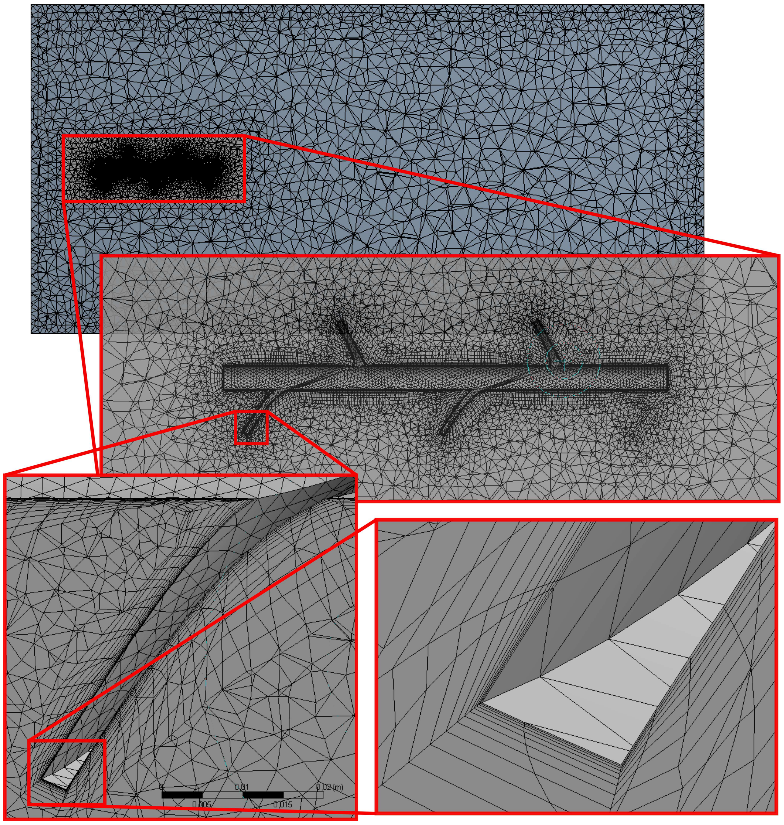

Figure 6: Zoom on the mesh refinement on the turbine surface.

this range of ω provides a TSR range between 0.125 and 1.5, that is sufficient to draw the performance curve of this kind of turbine. Each different configuration (reported in Table 6) was simulated for a total time of at least 10 s, with a time step of 0.02 s. Convergence iterations at each time step were run up to a relative error of 10^{-3} for mass conservation and 10^{-4} for the velocities, with a maximum number of 50 iterations for each time step. Every ten time steps, i.e. each 0.2 s, the torque generated by the fluid on the turbine M_t was evaluated as the torque due to both pressures and shear stresses acting on the whole turbine surface with respect to the turbine axis. Figures 7a-b illustrate the torque evolution in time for all simulations. It is evident that during the initial stage a peak evolves, this caused by the transient during which the fluid-structure interaction hydrodynamics develops from zero to a quasi-steady state. The time needed to achieve such

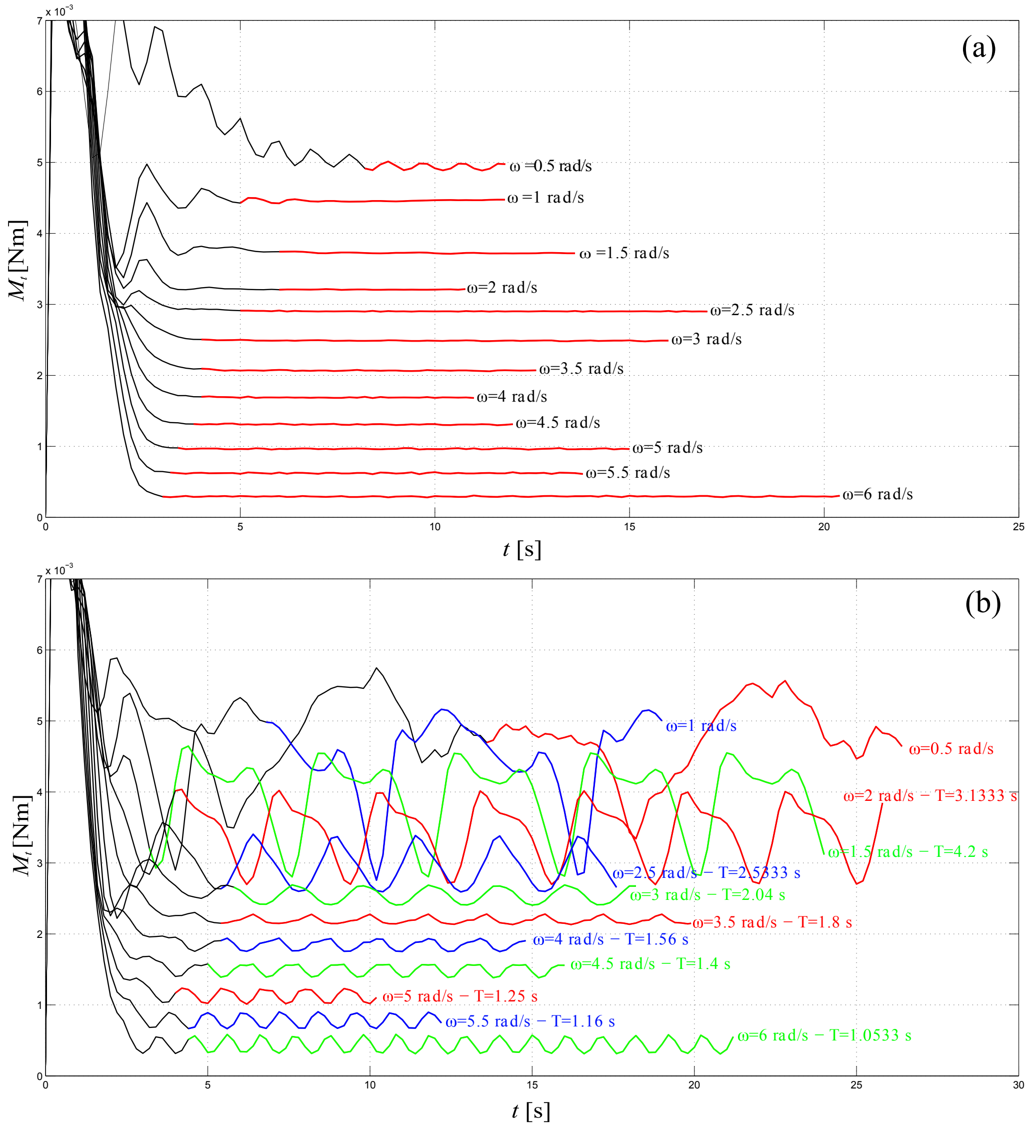

Figure 7: Evolution of the torque generated by the fluid on the turbine M_t, for each simulation, for the two configurations: a) aligned turbine ($\theta = 0°$); b) inclined turbine ($\theta = 10°$). At the end of each curve the angular velocity ω is reported, varied over the simulations. The coloured portions of each curve give the range used to evaluate the time-averaged torque used to calculate the performance coefficient. In panel b) the different colors are used to distinguish the curves of different simulations. For simulations with $\omega \geq 1.5$, both ω and T, evaluated over the coloured portion of the curve, are reported.

a quasi-steady condition (periodic oscillations in the inclined configuration) varied between 3 and 5 s. Results in this stage will be neglected in following analysis. Furthermore, for the inclined screw the torque evolution displays periodic oscillations for $\omega \geq 1.5$ rads^{-1} and the period of torque oscillation T was evaluated and reported in Figure 7b for each simulation. The period matches the relation $1/T = \omega/2\pi$, which is exactly the period of turbine rotation.

The periodic quasi-steady stage has been highlighted with colors in Figure 7 and such stage has been used to evaluate a time average of the torque $\bar{M}_t$. The achievement of the quasi-steady state has been defined in two different ways, depending on the shape of the signal. In case of a time-invariant signal, like those of Figure 7a, we required that the actual value of the variable would be within a tolerance of 10^{-4}Nm from the time-invariant value. For a periodic function, like those of Figure 7b, we implemented a Matlab routine to characterize the periodicity properties (period and amplitudes) and, starting from the end of the timeseries, moved backward in time until such properties remained within a tolerance of 10^{-4}Nm.

To check the sensivity of the results to the mesh, we executed five tests of the same simulation, varying the characteristics of the mesh. The studied simulation was the one identified with ID 0-3 in Table 6. A summary of each mesh characteristics is reported in Table 5. The results of the different

Table 5: Summary of the characteristics and results of the mesh sensivity analysis. MS4 corresponds to simulation ID 0-3 in Table 6.

Simulations	MS1	MS2	MS3	MS4	MS5	MS6
Mesh type	linear	linear	quadratic	linear	linear	linear
Max. mesh size [m]	0.5	0.05	0.05	$3 \cdot 10^{-2}$	$3 \cdot 10^{-2}$	$3 \cdot 10^{-2}$
Screw surface mesh size [m]	-	-	-	$3 \cdot 10^{-3}$ m	$1.5 \cdot 10^{-3}$	10^{-3}
Inflation - 1° layer thickness [m]	-	-	-	$1 \cdot 10^{-4}$ m	$1 \cdot 10^{-5}$	$1 \cdot 10^{-6}$
Inflation - $n°$ layers	-	-	-	12	12	12
Inflation - growth rate	-	-	-	1.4	1.4	1.4
$n°$ nodes	15847	37688	282855	157111	542271	1215726
$n°$ elements	84020	198767	198687	529599	1708176	3819192
$\bar{M}_t$ [Nm]	$2.46 \cdot 10^{-3}$	$2.45 \cdot 10^{-3}$	$2.47 \cdot 10^{-3}$	$2.49 \cdot 10^{-3}$	$2.55 \cdot 10^{-3}$	$2.63 \cdot 10^{-3}$
δ	-1.2 %	-1.5%	-1%	-	+2.5 %	+5.6 %
Y^+_{max}	42	40	34	3.4	3.9	3.9

simulations are compared in terms of both generated torque M_t, illustrated in Figure 8 and time-averaged torque $\bar{M}_t$, reported in Table 5. Since the simualtion $MS4$ is the reference simulation ID 0-3, the difference with the

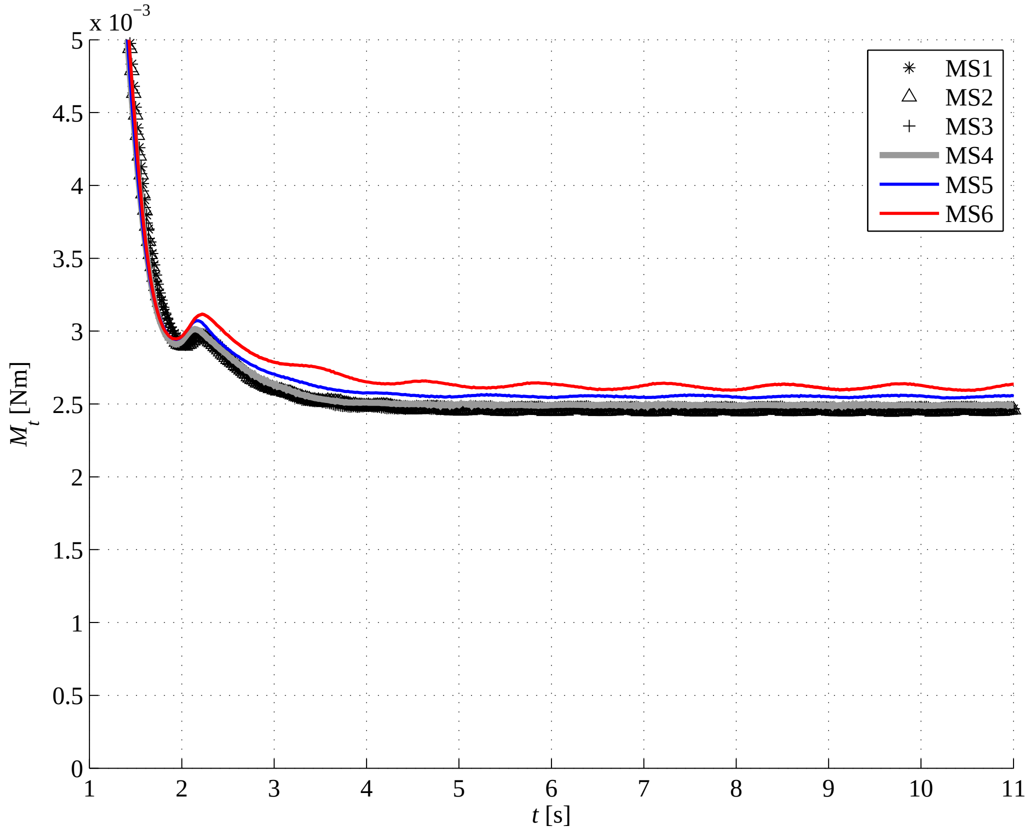

Figure 8: Results of mesh sensivity analysis. MS4 corresponds to simulation ID 0-3 in Table 6

reference simulation was evaluated with

$$\delta\left(MSi\right) = \frac{\bar{M}_t\left(MSi\right) - \bar{M}_t\left(MS4\right)}{\bar{M}_t\left(MS4\right)} \tag{8}$$

As reported in Table 5, all the results lie in a small range around the reference simulation ($\delta \in [-1.5\%, +5.6\%]$), this suggesting a small mesh sensivity. In addition, the refined simulations provided a time-averaged torque greater than the simulation analysed in this work. Also the inclined canfiguration was checked: the test with $\theta = 10°$ and $\omega = 2$ rads^{-1} was solved with a refined mesh, where the size assigned on the turbine surface was equal to $1.5 \cdot 10^{-3}$ m and the inflation had a first layer thickness equal to $1 \cdot 10^{-5}$ m, that increased for nine layers, with a growth rate of 1.4. The refined mesh had 616.415 nodes and 2.425.033. Also in this case, the simulation with the refined mesh provided a torque 5% larger than that of the simulation reported in this paper.

The influence of the time step on the simulation results was evaluated with the comparison of a reference (simulation ID 0-3 in Table 6) with two identical simulations, but with different time-step size: in the first, labelled with T1 in Figure 9, the time-step size was refined with $\Delta t = 0.01$, this providing an increase in the time-averaged generated torque (evaluated with Equation 8) of 1.2%; in the second, labelled with T2 in Figure 9, the time-step size was refined with $\Delta t = 0.002$ and the time-averaged generated torque increases of 3.7%. Also in this analysis, the simulations with refined time-step size pro-

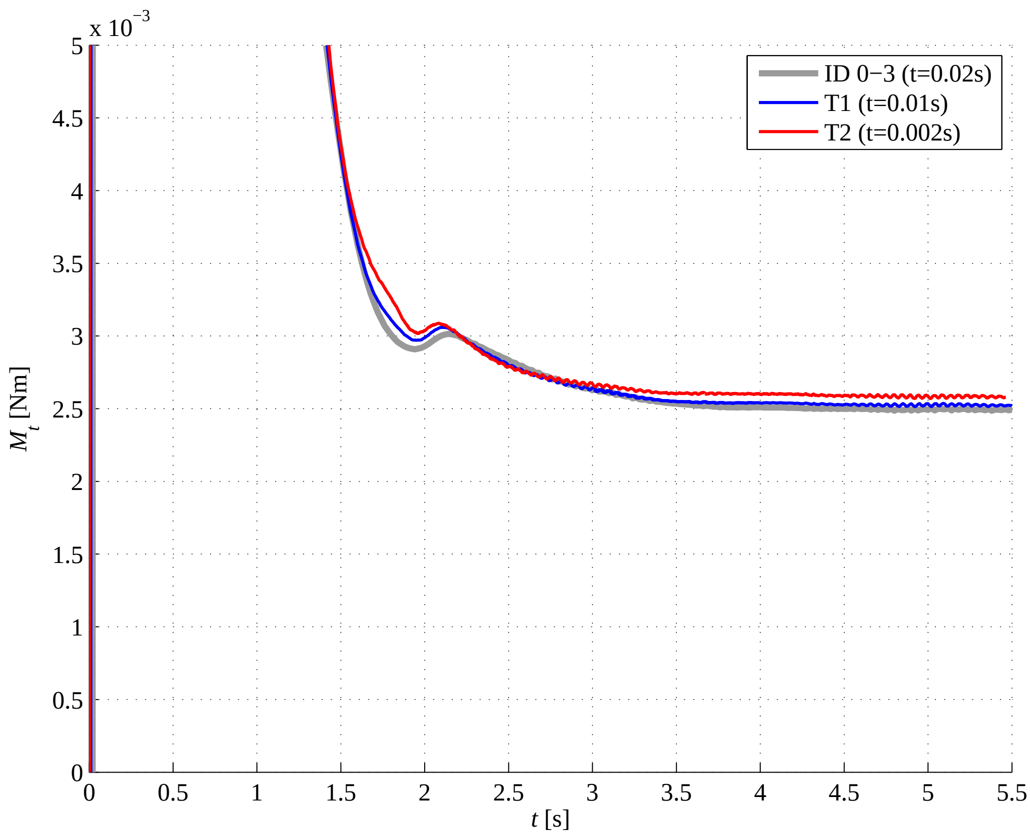

Figure 9: Results of time-step size sensivity analysis.

vided time-averaged torque in a small range around the reference simulation ($\delta \leq 5\%$), suggesting a small time-step size sensivity, and greater than the

time-averaged torque of the reference simulation.
However, such more accurate results, obtained with mesh or time-step size refinement, required a computational cost not acceptable for the entire numerical campain. Thus, the reported torque and the power and performance coefficient shown below are slightly understimated, but this does not invalidate the discussion of the results.
The power produced by the turbine has been evaluated as

$$P_t = \bar{M}_t \omega \tag{9}$$

The generated powers P_t are reported in Figure 10, showing that they are similar for the two configurations. Best fit of each configuration have been obtained using the Nonlinear Least Squares (NLS) regression, that solves nonlinear data-fitting problems in the least-squares sense with cubic function passing through the origin. The fit function evaluated are: $P_t = 3.22 \cdot 10^{-2}\omega^3 - \omega^2 + 5.2\omega$ mW for the aligned configuration and $P_t = 2.66 \cdot 10^{-2}\omega^3 - 0.95\omega^2 + 5.2\omega$ mW for the inclined configuration, where ω is in rads^{-1}.
The performance coefficient has, then, been evaluated as $C_{p,num} = P_t/P_f$, where the power of the flow P_f has been evaluated with equation (1) using the inflow-outflow velocity of the simulation, and it was equal to $P_{f,\theta=0}$ =31.42 mW for the aligned configuration and to $P_{f,\theta=10}$ =53.17 mW for the inclined configuration. The performance coefficients of the two configurations are shown in Figure 11. Also for the performence coefficient the best fit was obtained for each configuration, by using the Nonlinear Least Squares (NLS) regression. The fit function evaluated are: $C_p = 0.0656\mathrm{TSR}^3 - 0.5166\mathrm{TSR}^2 + 0.6653\mathrm{TSR}$ for the aligned configuration and $C_p = 0.0321\mathrm{TSR}^3 - 0.2881\mathrm{TSR}^2 + 0.3939\mathrm{TSR}$ for the inclined configuration. For comparison, also the laboratory results are reported in Figure 11.
Resuming the results, the values of the time-averaged torque $\bar{M}_t$, the generated power P_t and the numerical performance coefficient $C_{p,num}$ for each simulation are illustrated in Table 6.

5. Discussion and Conclusions

Results of laboratory experiments and numerical simulations showed that the performance coefficients of the hydrokinetic Archimedes are in line with the performances of the other hydrokinetic turbines, as reported in Table 7. For this reasons the Archimedes screw turbine has such efficiency characteristics that it can be assimilated to the hydrokinetic turbines actually in use

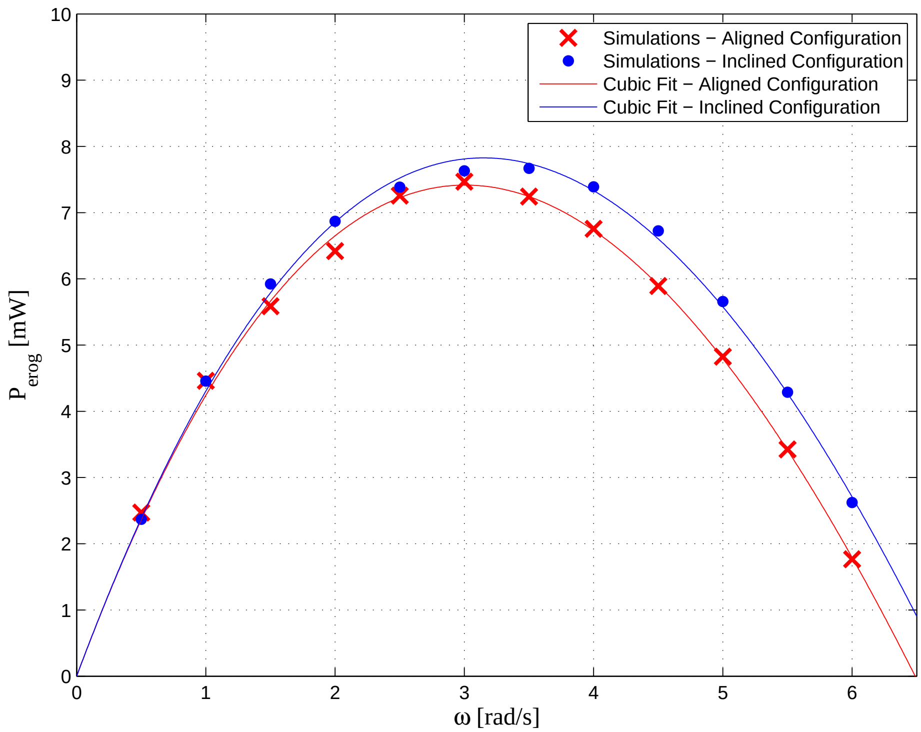

Figure 10: Generated power from numerical simulations, as function of the corresponding angular velocity ω.

Table 6: Summary of the conditions used for the numerical simulations and related results.

ID ($\theta - \omega$) grad-rads^{-1}	TSR [adim]	$\bar{M}_t$ [Nm]	P_t [mW]	C_p
0 - 0.5	0.125	$4.94 \cdot 10^{-3}$	2.47	0.079
0 - 1	0.25	$4.46 \cdot 10^{-3}$	4.46	0.142
0 - 1.5	0.375	$3.72 \cdot 10^{-3}$	5.59	0.178
0 - 2	0.5	$3.21 \cdot 10^{-3}$	6.42	0.204
0 - 2.5	0.625	$2.90 \cdot 10^{-3}$	7.23	0.231
0 - 3	0.75	$2.49 \cdot 10^{-3}$	7.47	0.238
0 - 3.5	0.875	$2.07 \cdot 10^{-3}$	7.24	0.231
0 - 4	1	$1.69 \cdot 10^{-3}$	6.76	0.215
0 - 4.5	1.125	$1.31 \cdot 10^{-3}$	5.89	0.188
0 - 5	1.25	$0.97 \cdot 10^{-3}$	4.83	0.154
0 - 5.5	1.375	$0.62 \cdot 10^{-3}$	3.42	0.109
0 - 6	1.5	$0.29 \cdot 10^{-3}$	1.76	0.056
10 - 0.5	0.125	$4.74 \cdot 10^{-3}$	2.37	0.045
10 - 1	0.25	$4.46 \cdot 10^{-3}$	4.46	0.084
10 - 1.5	0.375	$3.95 \cdot 10^{-3}$	5.92	0.111
10 - 2	0.5	$3.43 \cdot 10^{-3}$	6.87	0.129
10 - 2.5	0.625	$2.95 \cdot 10^{-3}$	7.38	0.139
10 - 3	0.75	$2.54 \cdot 10^{-3}$	7.63	0.144
10 - 3.5	0.875	$2.19 \cdot 10^{-3}$	7.67	0.144
10 - 4	1	$1.85 \cdot 10^{-3}$	7.39	0.139
10 - 4.5	1.125	$1.49 \cdot 10^{-3}$	6.72	0.126
10 - 5	1.25	$1.13 \cdot 10^{-3}$	5.66	0.106
10 - 5.5	1.375	$0.78 \cdot 10^{-3}$	4.29	0.081
10 - 6	1.5	$0.44 \cdot 10^{-3}$	2.62	0.049

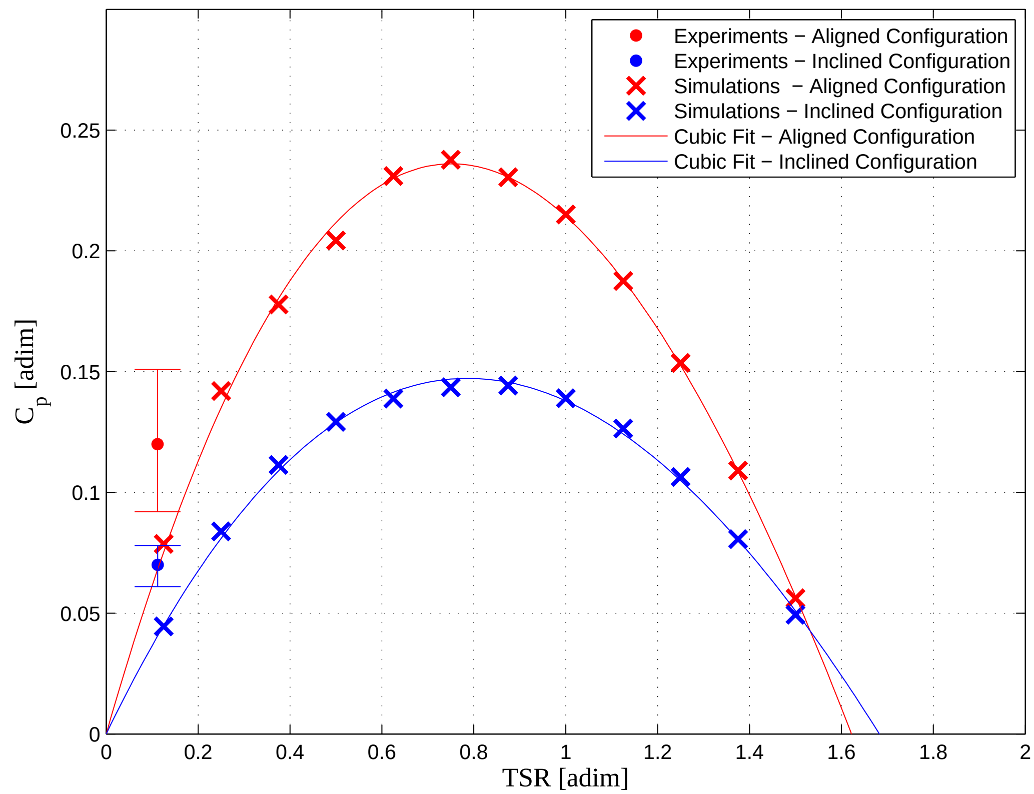

Figure 11: Power coefficient C_p as a function of the tip speed ratio for the laboratory experiments and for the numerical simulations.

for their ease of installation and low environmental impact.

Numerical and experimental results also state that the most efficient cofiguration is the aligned configuration. In fact, Figure 11 shows that the efficiency of the inclined configuration is smaller than that of the aligned configuration. This is due to the fact that the flow power available for the inclined configuration is greater ($P_{f,\theta=0}$ =31.42 mW, while $P_{f,\theta=10}$ =53.17 mW), but the produced power P_t is similar. In fact, the curves of generated power in the two different configurations (see Figure 10) have not highlighted important quantitative differences for $\omega \leq 3$. For $\omega \geq 3$ the inclined configuration provides a power slightly larger than that from the aligned configuration and also the velocity range of work increases (see the cubic fit curve in Figure 10). This is not quantitatively significant, but suggests a different interaction with the flow due to the inclination of the turbine.

Table 7: comparison of the maximum attainable performance coefficient for the Hydrokinetic Archimedes Turbine with the maximum attainable performance for some hydrokinetic turbines found in literature

Turbine type	C_p	Ref.
Axial flow turbine	0.43-0.45	[22, 24]
Rolling micro-turbines	0.55	[31]
Savonius	0.21-0.39	[32, 23]
Vertical-axis helical-bladed turbine	0.2-0.35	[33, 34]
Vertical Axis Autorotation Current Turbine	0.07	[35, 9]
Hydrokinetic Archimedes Turbine - Aligned configuration	0.238-0.264	-
Hydrokinetic Archimedes Turbine - Inclined configuration	0.144-0.167	-

In spite the performance coefficient obtained from the laboratory experiments provides only one point for each configuration in Figure 11, the most evident discrepancy is that the experimental efficiency is larger than that obtained numerically for the same TSR. This can be explained in view of the possible blockage, wall effects, that characterize the laboratory experiments: the flow confinement could increase the drag on the turbine and, as a consequence, the power generated by the turbine. However, the aim of numerical simulations was not at reproducing the experiments, but at : 1) extending the TSR range up to cover all the operative range of the Archimedes screw turbine and 2) removeing the effects of walls (blockage), support system and countweight system (e.g. frictional losses). Extending the TSR, numerical simulations provided the entire efficiency curves of the turbine in the anligned and inclined configuration (Figure 11), characterizing the turbine only.

Using the curves of performance coefficient of Figure 11, we can survey the feasibility of the proposed turbine. In a real case, we can suppose a generator of 500 W rated power, typically sold on the market, and search for the combination of turbine size (i.e. the radius R) and flow velocity v which ensure the work of the alternator. A parametric study is carried out, varying the flow velocity in the range $(0, 3)$ m/s and considering five different radius, between $R = 0.05$ m (as in the numerical simulation) and $R = 1$ m. Using a Matlab code, the available power P_f is evaluated for both aligned and inclined configuration and the genarated power P_t derived, considering the best performance, i.e. $TSR = 0.75$, which correspond to $\eta = 0.238$ in the aligned configuration and to $\eta = 0.144$ in the inclined configuration. The results of the analysis is reported in Figure 12. Focusing on the aligned configuration,

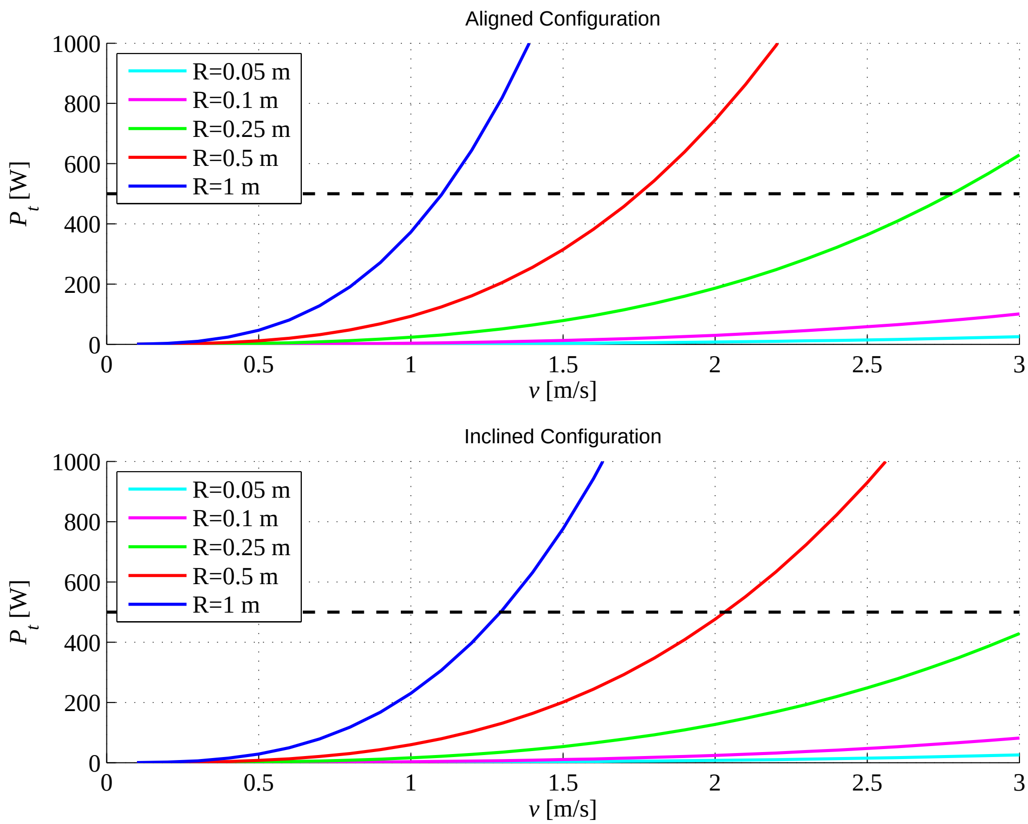

Figure 12: Power generated by Archimedean-Type Hydrokinetic turbines, with different radia R and for different water flow v.

it is evident that for the reference alternator functioning, a radius of at least 0.25 m s necessary, and a radius of 0.5 m is required for a flow velocity lower that 2 m/s. Similar considerations can be deduced from the results of the inclined configuration, even if in this configuration faster velocities are required to obtain the same P_t.

Efficiency curves also provide the TSR range in which the turbine is operative, i.e. for TSR$\leq$ 1.6, with a significant performance coefficient in the interval 0.5 $\leq$TSR$\leq$ 1. This is the same operative range of the Savonius rotor, showing similar efficiency (see Table 7 and [32, 23]), especially with the aligned configuration. The operative TSR range corresponds to low velocity regimes, which is an important characteristics for the compatibility with the ecosystem. In fact, if placed in river streams, low-velocity turbines induce

minor damages on the local fauna (i.e. fish).
Another interesting aspect is the periodicity of the power production, revealed by the numerical simulations for the inclined configuration (Figure 7b). This periodicity is less evident for the aligned configuration. An explaination to this aspect could related to the interaction of the turbine blades with the turbulence of the generated wake. If the turbine is aligned, we can suppose the generation of a wake downstream, rotating with the same axis of the turbine. In this condition, the interaction between the turbine blades and the wake does not vary with the rotation. Instead, if the turbine is inclined, the downstream wake would develop on a side of the rotation axis. In this case the rotation of the turbine changes periodically the position of the blades with respects to the wake, affecting the flow-turbine interaction and, subsequently, the generated power. This is supported by the fact that the generated torque period corresponds to the rotation period of the turbine T , i.e. the time required to achieve the same configuration blades/wake.
In conclusion:

- the performance coefficient of a ductless screw turbine have been evaluated, rigororusly, for a fixed geometry and have been found comparable with that of other hydrokinetic turbines characterized by the same velocity regime;
- the inclined configuration have been found worst than the aligned configuration, for its minor performance coefficient and for the periodicity of the generated torque, still requiring a detailed analysis;
- the proposed geometry can be used in real case application with large velocities or large radius.

For these reasons, Archimedes screw in the aligned configuration is a good candidate for the development of a device simple and cheap, minimizing the environmental impacts and reliable in variable water depth. Analysis is ongoing to further investigate the performances of this turbine in the inclined configuration.

References

[1] U. N. G. Assembly, Resolutions and decisions adopted by the general assembly during its seventieth session: Volume i 70/1 (2015). doi:10.18356/25329765-en.

[2] H. J. Vermaak, K. Kusakana, S. P. Koko, Status of micro-hydrokinetic river technology in rural applications: a review of literature, Renewable and Sustainable Energy Reviews 29 (2014) 625–633.

[3] K. Kusakana, H. Vermaak, Feasibility study of hydrokinetic power for energy access in rural south africa, in: Proceedings of the IASTED Asian conference, power and energy systems, 2012, pp. 433–438.

[4] K. Kusakana, H. J. Vermaak, Hydrokinetic power generation for rural electricity supply: Case of south africa, Renewable energy 55 (2013) 467–473.

[5] T. Price, D. Probert, Harnessing hydropower: A practical guide, Applied Energy 57 (23) (1997) 175–251. doi:10.1016/S0306-2619(97)00033-0.

[6] M. J. Khan, M. T. Iqbal, J. E. Quaicoe, River current energy conversion systems: Progress, prospects and challenges, Renewable and Sustainable Energy Reviews 12 (8) (2008) 2177–2193. doi:10.1016/j.rser.2007.04.016.

[7] M. J. Khan, G. Bhuyan, M. T. Iqbal, J. E. Quaicoe, Hydrokinetic energy conversion systems and assessment of horizontal and vertical axis turbines for river and tidal applications: A technology status review, Applied Energy 86 (10) (2009) 1823–1835. doi:10.1016/j.apenergy.2009.02.017.

[8] D. Kumar, S. Sarkar, A review on the technology, performance, design optimization, reliability, techno-economics and environmental impacts of hydrokinetic energy conversion systems, Renewable and Sustainable Energy Reviews 58 (2016) 796–813. doi:10.1016/j.rser.2015.12.247.

[9] A. C. Fernandes, A. B. Rostami, Hydrokinetic energy harvesting by an innovative vertical axis current turbine, Renewable Energy 81 (2015) 694–706. doi:10.1016/j.renene.2015.03.084.

[10] A. B. Rostami, M. Armandei, Renewable energy harvesting by vortex-induced motions: Review and benchmarking of technologies, Renewable and Sustainable Energy Reviews 70 (2017) 193–214.

[11] Archimedean screw hydro turbine, http://www.renewablesfirst.co.uk/hydropower/hydropower-learning-centre/archimedean-screw-hydro-turbine/ (accessed 24 october 2018).

[12] D. K. Okot, Review of small hydropower technology, Renewable and Sustainable Energy Reviews 26 (2013) 515–520. doi:10.1016/j.rser.2013.05.006.

[13] W. Schleicher, H. Ma, J. Riglin, Z. Kraybill, W. Wei, R. Klein, A. Oztekin, Characteristics of a micro-hydro turbine, Journal of Renewable and Sustainable Energy 6 (013119). doi:10.1063/1.4862986.

[14] A. Stergiopoulou, V. Stergiopoulos, E. Kalkani, Computational fluid dynamics study on a 3d graphic solid model of archimedean screw turbines, Fresenius Environmental Bulletin 23 (11) (2014) 2700–2706.

[15] A. Stergiopoulou, V. Stergiopoulos, E. Kalkani, Experimental and theoretical research of zero head innovative horizontal axis archimedean screw turbines, International Journal of Energy and Environment 6 (5) (2015) 471–478.

[16] A. Stergiopoulou, V. Stergiopoulos, E. Kalkani, Greece beyond the horizon of the era of transition: Archimedean screw hydropower development terra incognita, International Journal of Energy and Environment 6 (6) (2015) 527–536.

[17] A. Betz, Das maximum der theoretisch möglichen ausnützung des windes durch windmotoren, Zeitschrift für das gesamte Turbinenwesen 26 (1920) 307–309.

[18] A. Betz, The maximum of the theoretically possible exploitation of wind by means of a wind motor, Wind Engineering 37 (4) (2013) 441–446.

[19] M. Ragheb, A. Ragheb, Wind turbines theorythe betz equation and optimal rotor tip speed ratio. fundamental and advanced topics in wind power, dr. rupp carriveau (ed.), intech (2011).

[20] M. S. Guney, Evaluation and measures to increase performance coefficient of hydrokinetic turbines, Renewable and Sustainable Energy Reviews 15 (8) (2011) 3669–3675. doi:doi:10.1016/j.rser.2011.07.009.

[21] M. J. Khan, M. T. Iqbal, J. E. Quaicoe, Evaluation of maximum power point tracking in hydrokinetic energy conversion systems, The Journal of Engineering 11 (2015) 331–338. doi:10.1049/joe.2015.0157.

[22] W. C. Schleicher, J. D. Riglin, A. Oztekin, Numerical characterization of a preliminary portable microhydrokinetic turbine rotor design, Renewable Energy (76) (2015) 234–241.

[23] A. Kumar, R. P. Saini, Performance analysis of a savonius hydrokinetic turbine having twisted blades, Renewable Energy 108 (2017) 502–522. doi:10.1016/j.renene.2017.03.006.

[24] L. P. Chamorro, C. Hill, S. Morton, C. Ellis, R. E. A. Arndt, F. Sotiropoulos, On the interaction between a turbulent open channel flow and an axial-flow turbine, Journal of Fluid Mechanics 716 (2013) 658–670. doi:10.1017/jfm.2012.571.

[25] ANSYS Fluent Tutorial Guide, ANSYS, Inc. Release 18.0, (2017).

[26] B. Andersson, R. Andersson, L. Håkansson, M. Mortensen, R. Sudiyo, B. Van Wachem, Computational fluid dynamics for engineers, Cambridge University Press, (2011).

[27] F. R. Menter, Improved two-equation k-omega turbulence models for aerodynamic flows, NASA Technical Memorandum 103975 (1992).

[28] F. R. Menter, Two-equation eddy-viscosity turbulence models for engineering applications, AIAA journal 32 (8) (1994) 1598–1605. doi:10.2514/3.12149.

[29] Y. Hao, L. Tan, Symmetrical and unsymmetrical tip clearances on cavitation performance and radial force of a mixed flow pump as turbine at pump mode, Renewable energy 127 (2018) 368–376.

[30] Y. Liu, L. Tan, Tip clearance on pressure fluctuation intensity and vortex characteristic of a mixed flow pump as turbine at pump mode, Renewable energy 129 (2018) 606–615.

[31] V. Beran, M. Sedlcek, F. Marsk, A new bladeless hydraulic turbine, Applied energy (104) (2013) 978–983. doi:10.1016/j.apenergy.2012.12.016.

[32] K. Golecha, T. I. Eldho, S. V. Prabhu, Influence of the deflector plate on the performance of modified savonius water turbine, Applied Energy 88 (9) (2011) 3207–3217. doi:10.1016/j.apenergy.2011.03.025.

[33] P. K. Talukdar, V. Kulkarni, U. K. Saha, Field-testing of model helical-bladed hydrokinetic turbines for smallscale power generation, Renewable Energy (127) (2018) 158–167. doi:10.1016/j.renene.2018.04.052.

[34] A. N. Gorban, A. M. Gorlov, V. M. Silantyev, Limits of the turbine efficiency for free fluid flow, Journal of energy resources technology 123 (4) (2001) 311–317.

[35] A. C. Fernandes, A. B. Rostami, L. G. Canzian, S. M. Sefat, Vertical axis current turbine (vact) and its efficiency, in: ASME 2013 32nd International Conference on Ocean, Offshore and Arctic Engineering, American Society of Mechanical Engineers, 2013, pp. V008T09A051–V008T09A051.